


Article

The Removal of Tetracycline from Aqueous Solutions Using Peanut Shell Biochars Prepared at Different Pyrolysis Temperatures

Zhichao Shi ¹, Aowen Ma ¹, Yuanhang Chen ¹, Menghan Zhang ¹, Yin Zhang ¹, Na Zhou ¹, Shisuo Fan ^{1,*} and Yi Wang ^{2,*} 

¹ School of Resources and Environment, Anhui Agricultural University, Hefei 230036, China

² Key Laboratory of Agri-Food Safety of Anhui Province, Anhui Agricultural University, Hefei 230036, China

* Correspondence: fanshisuo@ahau.edu.cn (S.F.); wangyi@ahau.edu.cn (Y.W.);

Tel./Fax: +86-551-65786311 (S.F. & Y.W.)

Abstract: The pyrolysis temperature strongly affects the properties of the peanut shell biochar, and influences its adsorption behavior and mechanisms for contaminant removal in aqueous solutions. In this study, peanut shells were pyrolyzed at 400 °C and 700 °C to prepare two biochars (PSBC400 and PSBC700), which were then characterized using scanning electron microscopy/X-ray energy spectrum analysis, Brunauer–Emmett–Teller, elemental analysis, X-ray fluorescence, X-ray diffraction, Fourier transform infrared spectroscopy, and X-ray photoelectron spectroscopy. The adsorption behavior of typical tetracycline (TC) onto the biochars was investigated, and the potential adsorption mechanisms explored. The results show that compared with PSBC400, PSBC700 has a larger specific surface area and pore volume and contains higher levels of carbon and ash, but shows lower O, N, and H content. The hydrophilicity and polarity of PSBC700 is lower, but its aromaticity is higher. Furthermore, the mineral content of PSBC400 is higher than for PSBC700. The functional groups differ between PSBC400 and PSBC700, especially those containing C and O. The Elovich and two-compartment adsorption kinetic models are a good fit to the TC adsorption processes on both biochars, but the Langmuir adsorption isotherm model provides better results. The theoretical maximum adsorption capacities of TC onto PSBC700 and PSBC400 are 33.4346 mg·g⁻¹ and 26.4185 mg·g⁻¹, respectively. The main adsorption mechanisms of TC onto PSBC400 are hydrogen bonding and complexation, and are closely related to the functional groups and minerals found in PSBC400. In contrast, the main adsorption mechanisms of TC onto PSBC700 are pore filling and the π - π interaction, and are mainly determined by the surface area and graphitized carbon structure of PSBC700. In summary, effective biochar can be manufactured from peanut shell biomass and can be used to remove TC from aqueous solutions.

Keywords: peanut shells; biochar; pyrolysis temperature; tetracycline; adsorption mechanisms



Citation: Shi, Z.; Ma, A.; Chen, Y.; Zhang, M.; Zhang, Y.; Zhou, N.; Fan, S.; Wang, Y. The Removal of Tetracycline from Aqueous Solutions Using Peanut Shell Biochars Prepared at Different Pyrolysis Temperatures. *Sustainability* **2023**, *15*, 874. <https://doi.org/10.3390/su15010874>

Academic Editor: Luca Di Palma

Received: 23 November 2022

Revised: 27 December 2022

Accepted: 30 December 2022

Published: 3 January 2023



Copyright: © 2023 by the authors. Licensee MDPI, Basel, Switzerland. This article is an open access article distributed under the terms and conditions of the Creative Commons Attribution (CC BY) license (<https://creativecommons.org/licenses/by/4.0/>).

1. Introduction

With the rapid development of industrial medicine, a large number of antibiotics have been developed to treat various infectious diseases. Widespread use, and abuse, of antibiotics has resulted in the direct discharge of large quantities of waste antibiotics into the aquatic environment [1]. These antibiotics pose a serious threat to organisms because of their potential toxicity and potential to cause disease resistance [2]. Tetracycline (TC) is one of the most widely used antibiotics to cure several infectious diseases, and is frequently detected at high concentrations in aquatic environments where it may pose environmental hazards [3]. Therefore, the removal of TC from aquatic environments requires urgent attention.

Currently, TC is removed from the aquatic environment using membrane treatment, adsorption, advanced oxidation, electrochemical, and photocatalytic degradation tech-

niques [4]. However, adsorption remains a very important method for removing TC from natural waters and has the advantages of high efficiency, simplicity, environmentally friendliness, scalability, and ease of operation [5]. Selecting an optimal adsorbent is key to the successful application of the adsorption method. Activated carbon, resin, molecular sieves, and polymer materials are common adsorbents, but their high costs prevent their widespread application [6]. There is a need to find widely available, low cost, and environmentally friendly substitute biomass-based adsorption materials. Biochar is a promising cost-effective alternative adsorbent and has attracted much attention recently due to its large specific surface area, porous structure, and surface functional groups and minerals [7–13]. The properties of biochars rely heavily on the nature of the feedstock and the means of pyrolysis, especially the pyrolytic temperature [14,15].

China is currently the largest peanut-producing country in the world, with an annual production of about 3.14 million tons, and peanut shells have become an abundant biomass resource [16,17]. Peanut shells can be used as a substrate, fertilizer, fuel, animal feed, and in the preparation of activated carbon [18]. Preparation of biochar provides a new way to utilize this resource. Peanut shell biochar, or modified peanut shell biochar, has been used as an adsorbent for the removal of pollutants from wastewater, including pesticides, [19], antibiotics [20,21], heavy metals [22,23], dyes [24], nitrogen, and phosphorus [25], clearly demonstrating its effectiveness

Previous studies show that the pyrolysis temperature significantly affects the physicochemical properties of the biochar produced, further influencing the adsorption mechanisms of pollutants [26]. Pyrolysis temperature expressly affects the chemical composition, functional groups, pore structure, and crystallographic structure of a biochar and these changes can affect the binding properties of contaminants to the biochar [26–29]. For example, Dai et al. studied the adsorption of TC in aqueous solution by biochar derived from waste *Auricularia auricula* dregs under different pyrolysis temperatures [30]. Kim et al. investigated the adsorptive removal of TC from aqueous solution by maple-leaf-derived biochar prepared at different temperatures [31]. Zhang et al. investigated the characteristics of tetracycline adsorption by cow manure biochar prepared at different pyrolysis temperatures [32]. Choi et al. performed the adsorption behavior of tetracycline onto *Spirulina* sp. (microalgae)-derived biochars produced at different temperatures [33]. The above research confirmed that the specific surface area, pore structure, surface functional groups, and microstructure of the biochars derived from various pyrolysis were different, then influencing their adsorption performance towards TC. However, very few studies have reported specifically on the effects of pyrolysis temperature on the physicochemical properties of peanut shell biochar. In addition, the influence of pyrolysis temperature on the adsorption mechanism of TC by peanut shell biochar is still unclear.

In this work, peanut shells were converted to biochars under pyrolysis temperatures of 400 °C and 700 °C (PSBC400 and PSBC700, respectively). The biochars obtained were characterized using scanning electron microscopy/X-ray energy spectrum analysis (SEM/EDS), Brunauer–Emmett–Teller (BET), elemental analysis (EA), X-ray fluorescence (XRF), X-ray diffraction (XRD), Fourier transform infrared spectroscopy (FTIR), and X-ray photoelectron spectroscopy (XPS). The adsorption behaviors of TC onto the two biochars were investigated, including their adsorption kinetics and isotherms. Finally, the potential adsorption mechanisms of TC onto biochar were investigated. The results provide a reference for the utilization of peanut shells as biochar feedstock, and technical support for their use in removing TC from aquatic environments.

2. Materials and Methods

2.1. Materials

Peanut shells were collected from a factory in the suburb of Hefei, Anhui Province, China. The peanut shells were soaked in tap water to wash dust and impurities from the surface, then repeatedly washed with deionized water, dried at 80 °C in an oven, and then powdered for further use.

Tetracycline (TC, $C_{22}H_{24}N_2O_8$) was purchased from the Shanghai Yuanye Biological Co., Ltd., Shanghai, China. The other chemical reagents used were analytically pure and were obtained from the Sinopharm Chemical Reagent Company Ltd., Shanghai, China.

2.2. Biochar Preparation

Two batches of powdered peanut shell were placed into quartz boats, and then into a tubular muffle furnace (OTF-1200X, Hefei Kejing Mater. Technology Company., Ltd., Hefei, China) for pyrolysis. The pyrolysis temperatures were set at 400 °C and 700 °C for each batch, with a heating rate of 5 °C·min⁻¹. Once the desired temperature was reached, the samples were kept at the target temperature for 2 h. The whole pyrolysis process was conducted in an N₂ atmosphere with a flow rate of 100 mL·min⁻¹. The pyrolyzed solid was removed after the tubular furnace had cooled to room temperature. The two solids obtained were ball milled for 2 min to produce uniform samples.

2.3. Batch Adsorption Experiment

2.3.1. Adsorption Kinetics

Two 250 mL samples of 50 mg·L⁻¹ TC solution were placed into 250 mL conical flasks, and 0.02 g of each biochar was added. The flasks were placed into an oscillator at a temperature of 25 °C, and an oscillation speed of 180 r·min⁻¹. The samples were collected at intervals from 0–600 min. The samples were filtered through 0.45 μm filters, and measured using a UV–visible spectrophotometer at 358 nm (UV-5100B, Metash, Shanghai, China).

The amount of TC absorbed onto the biochar (q_t , mg·g⁻¹) after an adsorption process contact time, t , was calculated as shown in Equation (1). Pseudo-first-order (PFO) (Equation (2)), pseudo-second-order (PSO) (Equation (3)), Elovich (Equation (4)), and two-compartment (Equation (5)) models were used to fit the adsorption kinetics process [34,35].

$$q_t = \frac{(C_0 - C_t)V}{m} \quad (1)$$

$$q_t = q_e(1 - \exp(-k_1 t)) \quad (2)$$

$$q_t = \frac{q_e^2 k_2 t}{1 + q_e k_2 t} \quad (3)$$

$$q_t = (1/\beta) \ln(\alpha\beta) + (1/\beta) \ln(t) \quad (4)$$

$$q_t = q_e [1 - (F_{fast} e^{-k_{fast} t} + F_{slow} e^{-k_{slow} t})] \quad (5)$$

where: C_0 and C_t are the initial concentration and contact time of TC in the solution (mg·L⁻¹), respectively; V is the volume of TC solution (L); m is the mass of biochar (g); q_t and q_e are the adsorption capacity of TC at time t and at equilibrium (mg·g⁻¹), respectively; t is adsorption time (min); k_1 and k_2 are the PFO and PSO rate constants (min⁻¹, g·mg⁻¹·min⁻¹), respectively; α is the initial adsorption coefficient (g·mg⁻¹·min⁻¹); β is the desorption rate constant (g·mg⁻¹); F_{fast} is the proportion of the fast adsorption stage; F_{slow} is the proportion of the slow adsorption stage (where the sum of F_{fast} and F_{slow} is equal to 1); and k_{fast} and k_{slow} are the rate constants of the fast and slow reactions (min⁻¹), respectively.

2.3.2. Adsorption Isotherms

A series of 20 mL TC solutions with a concentration of 10–50 mg·L⁻¹ were placed in brown glass bottles. A 0.02 g biochar sample was added to the solution to keep a solid/liquid ratio of 1 g·L⁻¹. The bottles were placed into an oscillator at a temperature of 25 °C, and an oscillation speed of 180 r·min⁻¹. After oscillation, the mixtures were centrifuged at 5000 rpm (3913× g) for 10 min, filtered through a 0.45 μm filter, and the absorbance of the solutions was analyzed to calculate the TC concentrations.

At the equilibrium time, the amount of TC absorbed onto the biochar (q_e , mg·g⁻¹) was calculated as shown in Equation (6). Langmuir (Equation (7)) and Freundlich (Equation

(8)) models were used to fit the adsorption process [36]. The Langmuir model explains the ideal monolayer adsorption onto a homogeneous surface, while the Freundlich model expresses the non-ideal multilayer adsorption onto a non-homogeneous surface [37].

$$q_e = \frac{(C_0 - C_e)V}{m} \quad (6)$$

$$q_e = \frac{q_{\max}k_L C_e}{1 + k_L C_e} \quad (7)$$

$$q_e = K_f C_e^{1/n} \quad (8)$$

where k_L is Langmuir constant ($L \cdot g^{-1}$); q_{\max} is the maximum adsorption capacity ($mg \cdot g^{-1}$); K_f is the Freundlich constant ($mg \cdot g^{-1} / (mg \cdot L^{-1})^n$); and $1/n$ is a constant reflecting adsorption affinity.

2.4. Biochar Characterization

The surface morphology and elemental composition of the two biochars were examined using SEM (S-4800, Hitachi, Japan) and EDS (X-Max, Oxford Instruments, UK). The pore structure and specific surface area (SSA) of the biochars were characterized using a Micromeritics TriStar II 3020 with an N_2 adsorption–desorption isotherm at 77.3 K. The C, H, and N contents were determined using an elemental analyzer (Elemental analyzer, Vario, Germany). Ash content was determined by calcination at 700 °C for 2 h, and the O content was obtained by difference subtraction ($O = 100\% - (C - N + H + S + Ash)$). Chemical analyses of biochars were determined by X-ray fluorescence (XRF-1800, Shimadzu, Japan) using calibration carried out by the manufacturer for the analysis of basic materials. The surface functional groups of the biochars were analyzed using Fourier transform infrared spectroscopy (Nicolette is 50, Thermo Fisher, Waltham, MA, USA). The phase structures of the biochars were analyzed using XRD with Cu K α radiation source within the scanning angle range of 5°–80° at a scanning rate of 2° min^{−1} (Bruker D8 Advance, Germany). The functional groups present on the surfaces of the biochar particles and the elemental composition of the top surface layers (3–5 nm) were measured using a Thermo-VG Scientific ESCALAB 250 Xi spectrometer (Thermo Scientific, Waltham, MA, USA).

3. Results and Discussion

3.1. Biochar Characterization

Figure 1 shows the SEM/EDS images of the two biochars. No obvious pore structure is found in PSBC400, which retains the surface morphology of pristine peanut shells. The main elements include C, O, Ca, Si, Mg, and Al, as both organic and mineral components. In PSBC700, some fragments and pore structures are visible since the high pyrolysis temperature results in organic matter decomposition and gas release [38]. Both biochars consist largely of C and O, with the C content accounting for more than 90% of the total mass.

The N_2 adsorption–desorption curve and pore size distribution of the biochars are shown in Figure 2. It is shown that PSBC400 and PSBC700 present pseudo-type-IV curve with a H3 hysteresis loop, which shows mesoporous structure, with pore sizes of 2–10 nm. The pore structure parameters of both biochars are shown in Table 1. The surface area and pore volume of PSBC700 are 193.6540 m²·g^{−1} and 0.128353 cm³·g^{−1}, and are 26.0 and 8.8 times greater than PSBC400, respectively. The average pore size of PSBC700 is much smaller than PSBC400, which is more conducive to the diffusion adsorption of pollutants.

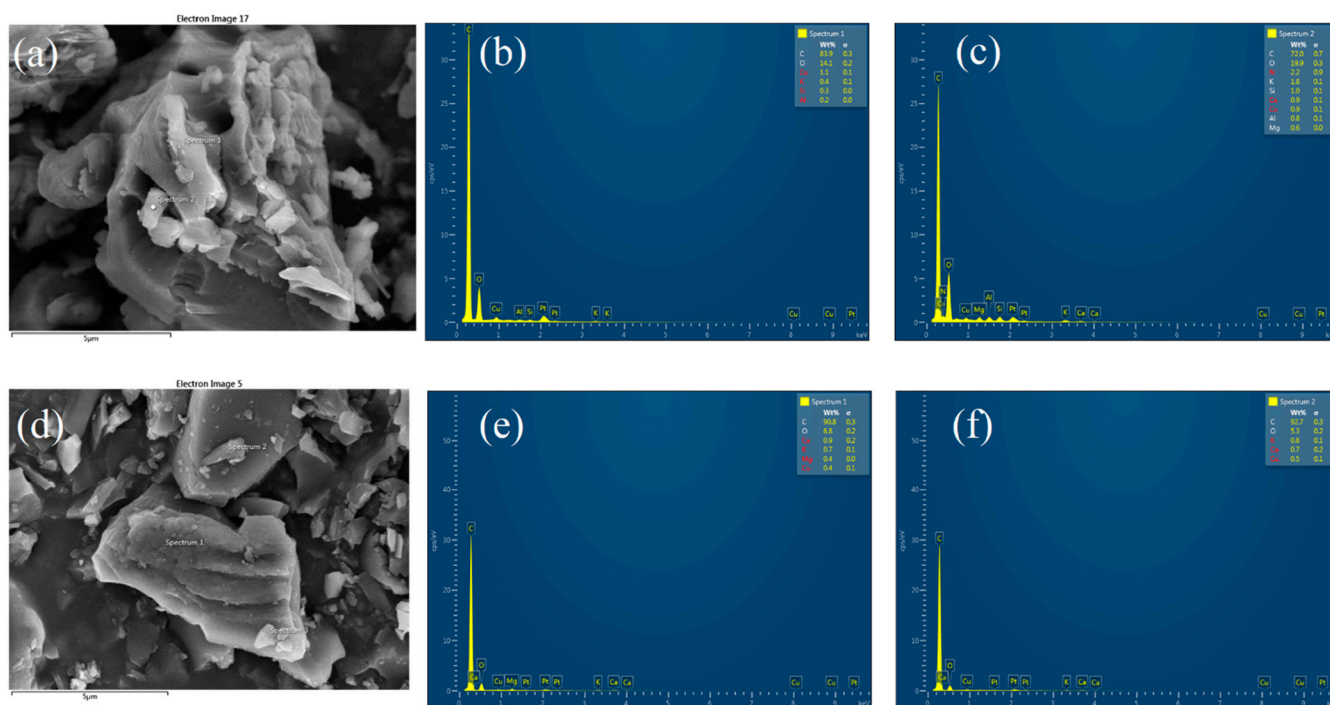


Figure 1. SEM and EDS images of biochars, PSBC400 (a–c); PSBC700 (d–f).

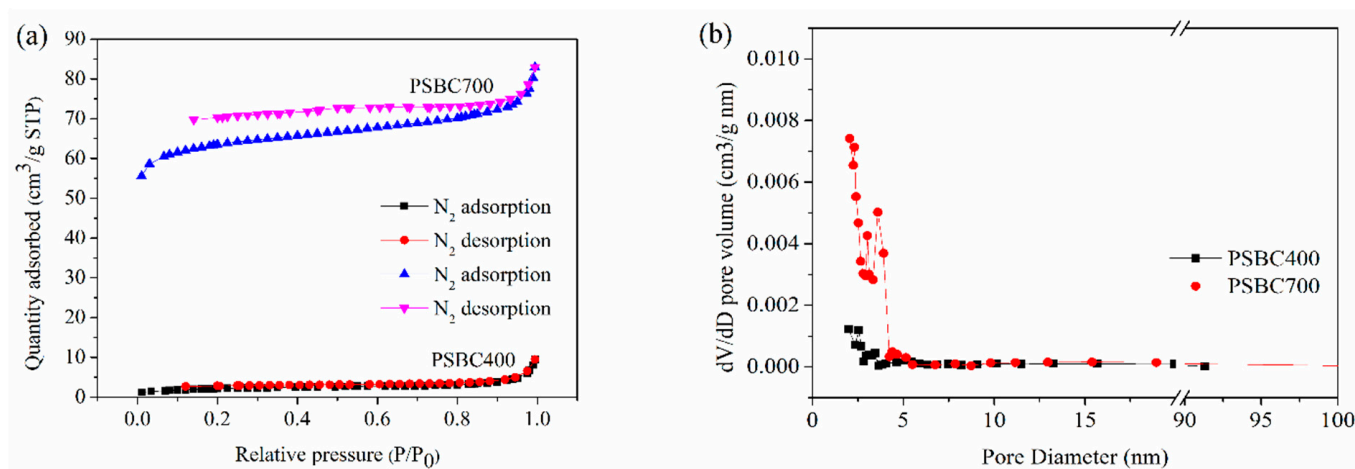


Figure 2. N₂ adsorption–desorption curve (a) and pore size distribution (b) of biochars.

Table 1. Pore structure parameters of biochars.

Parameters	Unit	PSBC400	PSBC700
Surface area (S_{BET})	$m^2 \cdot g^{-1}$	7.4290	193.6540
Total volume (V_{Total})	$cm^3 \cdot g^{-1}$	0.014633	0.128353
Average pore size (L_0)	nm	7.8791	2.6512

The elemental and ash contents of the biochars and their calculated atomic ratios are shown in Table 2. PSBC700 has a higher C and ash content, but lower N, H, and O content than PSBC400, especially the H and C content. The lower O and H contents of PSBC700 are probably due to dehydration, dehydrogenation, and deoxygenation reactions caused by the higher pyrolysis temperature [39]. The atomic ratios of H/C, O/C, and (O + N)/C are recognized indices for aromaticity, hydrophily, and polarity, respectively [40]. The smaller the H/C atomic ratio, the higher the aromaticity of a biochar. The higher the (N + O)/C

atomic ratio, the higher the polarity [41]. In this study, bulk aromaticity of the biochars increases, while hydrophily and polarity decrease with increased pyrolysis temperature, as indicated by the decreasing H/C, O/C, and (O + N)/C ratios.

Table 2. Element, ash content, and atomic ratios of biochars.

Biochar	C	N	H	O	Ash	H/C	O/C	(N+O)/C
PSBC400	67.624	1.918	4.208	18.095	8.155	0.062	0.268	0.296
PSBC700	80.334	1.561	1.910	7.049	9.146	0.024	0.088	0.107

The chemical compositions of the biochars were determined using XRF and are shown in Table 3. Compared with PSBC400, the higher pyrolysis temperature of PSBC700 increases the C content and decreases the N content. The relative content of Si, K, Ca, Al, Fe, Na, and S in PSBC400 is greater than in PSBC700. Conversely, the Mg and P content of PSBC400 is less than in PSBC700. In general, the mineral content of biochar increases with increasing pyrolysis temperature because the organic biomass constituents, including cellulose, hemicelluloses, and lignin are, to a large extent, converted and released in the form of volatiles and gases while the much less volatile mineral compounds, such as Mg, Ca, and P, remain, and, therefore, become concentrated in the biochar [42]. In addition, the minerals in high temperature biochars may also increasingly crystallize and become less soluble, especially above 500 °C, and are, therefore, less effective as adsorption binding sites for pollutants [42].

Table 3. Main chemical compositions in biochars based on XRF (%).

Components	PSBC400	PSBC700
C	72.9068	82.6192
N	15.7178	7.6861
SiO ₂	3.7452	2.8873
K ₂ O	2.0381	1.6741
CaO	1.4887	1.3506
MgO	0.9	1.0132
Al ₂ O ₃	0.7953	0.6823
P ₂ O ₅	0.7263	1.1234
SO ₃	0.6038	0.4692
Fe ₂ O ₃	0.4717	0.2418
Na ₂ O	0.2812	0.112
TiO ₂	0.0834	0.0359
Cr ₂ O ₃	0.0797	0.0197
Cl	0.0594	0.0282
MnO	0.0374	0.025
NiO	0.0288	0.0101
Co ₂ O ₃	0.0214	—
CuO	0.0151	0.0075

The XRD patterns of the biochars are shown in Figure 3a. Typical diffraction peaks of SiO₂ are observed in these peanut shell biochars. Increased pyrolysis temperature results in a weakened intensity of the SiO₂ diffraction peak, which may be ascribed to the decrease in SiO₂ content or the formation of Si/C. A wide diffraction peak at about 23° is observed in the biochars, indicating the presence of amorphous carbon structures. The diffraction peak at 44° (100 planes) in PSBC700 corresponds to crystalline graphite carbon, indicating that high temperature pyrolysis is beneficial for the formation of graphite structure in the biochar [43].

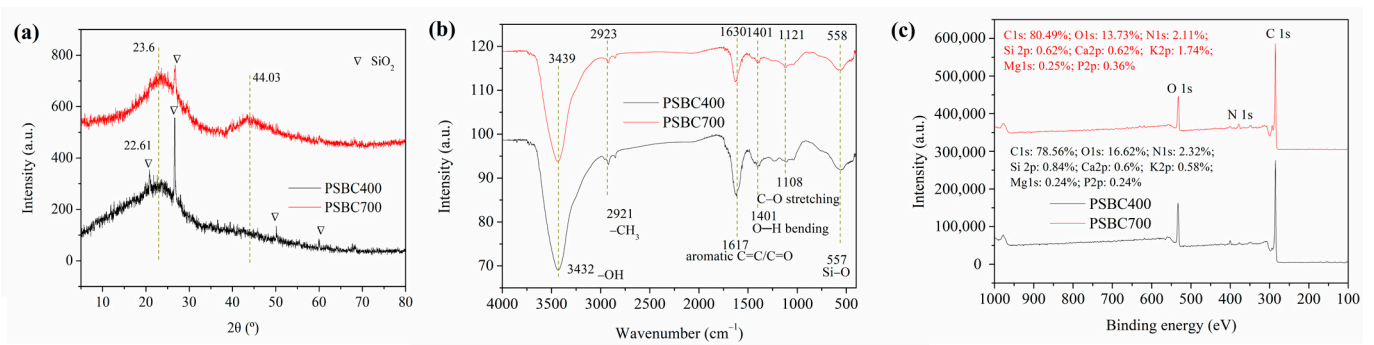


Figure 3. XRD (a), FTIR (b), and XPS (c) of biochars.

The FTIR spectra of the biochars are presented in Figure 3b. PSBC400 and PSBC700 contain many functional groups, such as $-\text{OH}$, $-\text{CH}_3$, aromatic $\text{C}=\text{C}/\text{C}=\text{O}$, $\text{O}-\text{H}$ bending, $\text{C}-\text{O}$ stretching, and $\text{Si}-\text{O}$ [21,38]. Increased pyrolysis temperature leads to shifts in some groups, such as $1617\text{ cm}^{-1} \rightarrow 1630\text{ cm}^{-1}$, $1108\text{ cm}^{-1} \rightarrow 1121\text{ cm}^{-1}$ for aromatic $\text{C}=\text{C}/\text{C}=\text{O}$ and $\text{C}-\text{O}$ stretching, respectively. The change in functional groups is attributed to the dehydration, dehydrogenation, and deoxygenation reactions at the elevated temperatures [39,44,45].

The XPS results of the two biochars are shown in Figure 3c. The elements C, N, and O are detected on the biochar surfaces. Furthermore, other minerals, including Si, Ca, K, Mg, and P, are also found on the biochar surfaces. Compared with PSBC400, the C content is higher in PSBC700, but the O and N content is lower, consistent with the elemental analysis results. Furthermore, mineral element contents, such as Ca, K, and Si, also change slightly.

Peak fitting of the C1s, N1s, and O1s of the biochars are shown in Figure 4. The C1s spectrum of PSBC400 shows characteristic peaks at 284.80 and 286.28 eV, corresponding to $\text{C}-\text{C}/\text{C}-\text{H}$ and $\text{C}-\text{O}-\text{C}$ [16], respectively. However, the C1s peaks for PSBC700 occur at 284.77 eV (for $\text{C}-\text{C}/\text{C}-\text{H}$), 285.49 eV (for $\text{C}-\text{O}-\text{C}$), and 287.91 eV (for $\text{O}-\text{C}=\text{O}$). The types of N found in PSBC400 and PSBC700 include pyridinic-N and pyrrolic-N [46]. The O1s photoelectron spectrum of PSBC400 can be resolved into two signals, which are attributed to $\text{C}=\text{O}$ (531.78 eV) and $\text{C}-\text{O}$ (533.37 eV) [47,48]. The chemical composition of the O1s XPS spectra of PSBC700 shows two different peaks at ~ 531.46 and ~ 532.86 eV for $\text{C}=\text{O}$ and $-\text{OH}$, respectively [49]. The pyrolysis temperature, therefore, significantly affects the carbon structure and oxygen-containing functional groups in the biochars produced. The changes in carbon structure is consistent with the XRD analysis, while the changes in functional groups are the same as in the FTIR analysis.

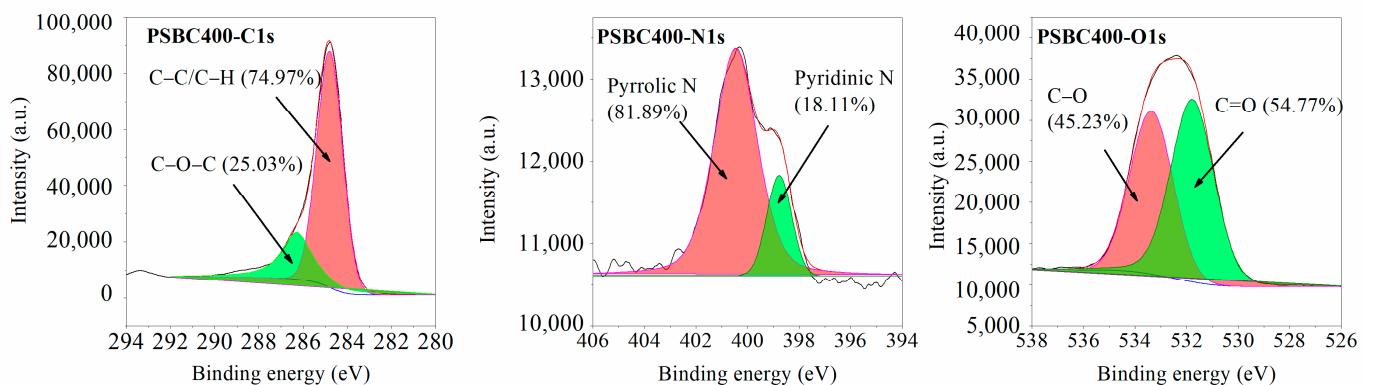


Figure 4. Cont.

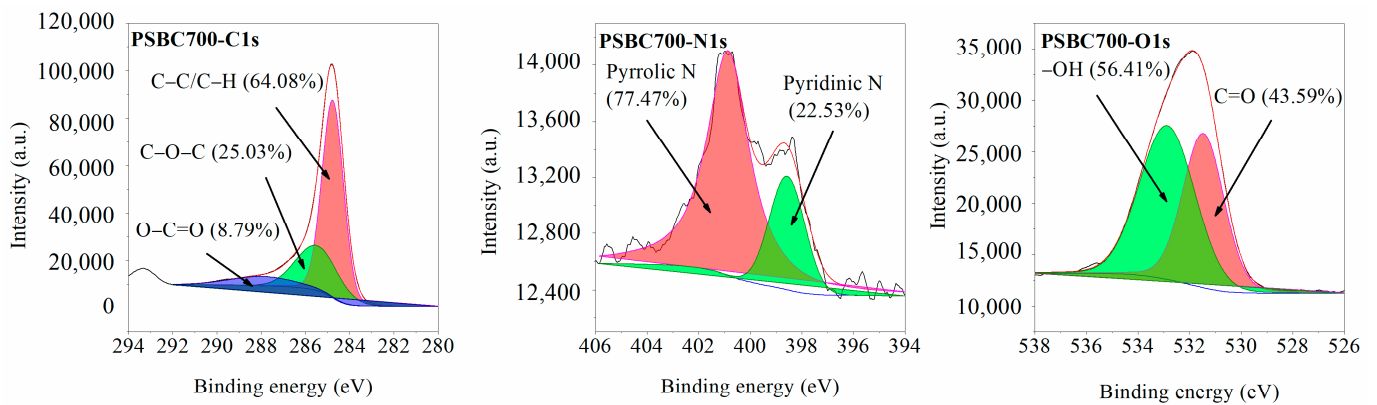


Figure 4. XPS spectra analysis of biochars.

3.2. Adsorption Behavior of TC on Biochars

3.2.1. Adsorption Kinetics

The adsorption kinetics of TC onto the biochars are presented in Figure 5. The adsorption of TC onto the biochars first increases and then stabilizes with increasing contact time [40]. The TC removal rates by PSBC400 and PSBC700 at 5 and 30 min are 59% and 75%, and 77% and 81%, respectively. Hence, the majority of the removal of TC by the biochars occurs during the initial stage of the adsorption process [50].

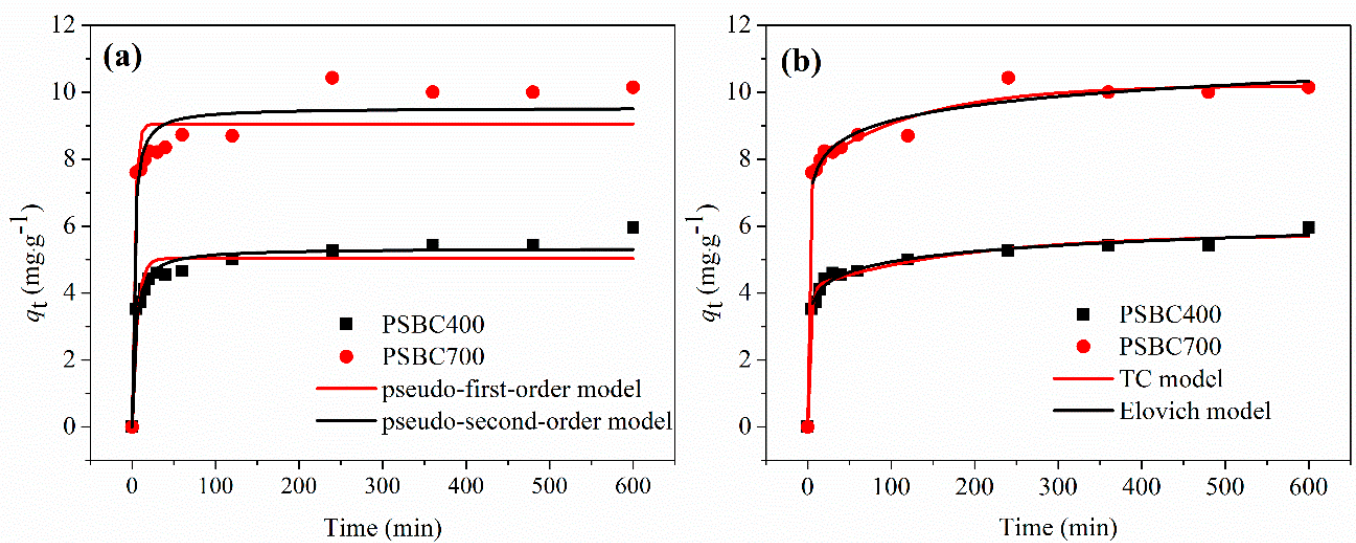


Figure 5. Adsorption kinetics of TC by biochars, pseudo-first-order and pseudo-second-order model (a); Elovich and two-compartment model (b).

The parameters of TC adsorption by the biochars, fitted by the various kinetics models, are shown in Table 4. The PSO model provides a better description of the TC adsorption process than the PFO model. The correlation coefficient (R^2) of the PSO model is greater than that of the PFO model, and the obtained adsorption capacity of the PSO model is closer to the practical adsorption amount. Generally, the PSO model provides a good fit to all the experimental data, implying that chemical interactions are involved in the adsorption process, and that strong interactions involving valence forces sharing or exchanging electrons occurs between TC and the biochar [51]. In addition, the PSO model also explains the external liquid film diffusion, surface adsorption, and intra-particle diffusion processes coexisting during adsorption, and fully and accurately describes the adsorption process [52].

Table 4. Fitting parameters of adsorption kinetics of TC onto biochars.

Biochar	Pseudo-First-Order Model			Pseudo-Second-Order Model		
	$q_e/(\text{mg}\cdot\text{g}^{-1})$	k_1/min^{-1}	R^2	$q_e/(\text{mg}\cdot\text{g}^{-1})$	$k_2/\text{g}(\text{mg}\cdot\text{min}^{-1})$	R^2
PSBC400	5.03558	0.15985	0.88435	5.33639	0.04938	0.9565
PSBC700	9.05284	0.29732	0.88186	9.53403	0.0496	0.9386

Biochar	Elovich model			Two-compartment model					
	a	β	R^2	$q_e/(\text{mg}\cdot\text{g}^{-1})$	F_{fast}	F_{slow}	k_{fast}	k_{slow}	R^2
PSBC400	290.43196	2.2472	0.9909	5.7517	0.7235	0.2765	0.3217	0.0055	0.9800
PSBC700	6677.55413	1.51165	0.99215	10.2061	0.7504	0.2496	0.7690	0.00799	0.9866

The Elovich equation has been used to predict a number of transport-limited reaction mechanisms, including bulk and surface diffusion [53,54]. In this study, the Elovich equation provides the best fit to the experimental data ($R^2 > 0.99$), suggesting that TC adsorption onto the biochars is predominantly mediated by chemical interactions taking place at the strongly heterogeneous biochar surfaces [55,56].

The two-compartment first-order model divides the adsorption process into two parts, namely, the fast adsorption stage and the slow adsorption stage [37]. In this study, the good fit of the two-compartment model (R^2 : 0.9800 and 0.9866, for PSBC400 and PSBC700, respectively) confirms the two-stage nature of the adsorption of TC onto the two biochars, as described in Section 3.2.1. Specifically, TC is rapidly absorbed by PSBC400 and PSBC700 within 15 min, reaching 72.35% and 75.04% of the total adsorption capacity, respectively. The adsorption process slows in the following 585 min, during which time only an additional 27.65% and 24.96% of the total adsorption capacity is achieved by PSBC400 and PSBC700, respectively. In addition, the k_{fast} values for PSBC400 and PSBC700 are larger than those of k_{slow} . Based on the analysis of characterization, the fast adsorption stage of PSBC400 relates to its functional groups and minerals. However, the fast adsorption stage of PSBC700 is due to its larger surface area and graphitic aromatic structure.

3.2.2. Adsorption Isotherms

Adsorption isotherms can describe the equilibrium distribution of TC molecules between the adsorbent and the solution. Figure 6 shows the adsorption isotherms of TC on the two biochars. When the equilibrium concentration increases, the equilibrium adsorption capacity (q_e) for TC first increases sharply, then increases slightly, and finally reaches the equilibrium point, as expected.

The parameters obtained from the adsorption isotherm models are shown in Table 5. The theoretical maximum adsorption capacity of TC onto PSBC400 and PSBC700 reaches $26.4185 \text{ mg}\cdot\text{g}^{-1}$ and $33.4346 \text{ mg}\cdot\text{g}^{-1}$, respectively. The affinity between PSBC700 and TC is greater than that between PSBC400 and TC because of its high k_L value. Based on the K_F and n values, PSBC700 shows a greater ability to adsorb TC than PSBC400. Compared with the pristine biochar of other feedstock in Table S1, the adsorption capacity of TC on peanut shell biochar is larger and more apparent. However, compared with the modified biochars in Table S2, the adsorption amount of peanut shell biochar for TC is relatively low due to the deficiency of abundant adsorption sites.

Table 5. Fitting parameters of adsorption isotherms of TC onto biochars.

Biochar	Langmuir			Freundlich		
	$q_{\text{max}}/(\text{mg}\cdot\text{g}^{-1})$	$k_L/(\text{L}\cdot\text{mg}^{-1})$	R^2	K_F	n	R^2
PSBC400	26.4185	0.03916	0.99057	2.63807	2.09028	0.97974
PSBC700	33.4346	0.05743	0.97443	4.4245	2.27244	0.92564

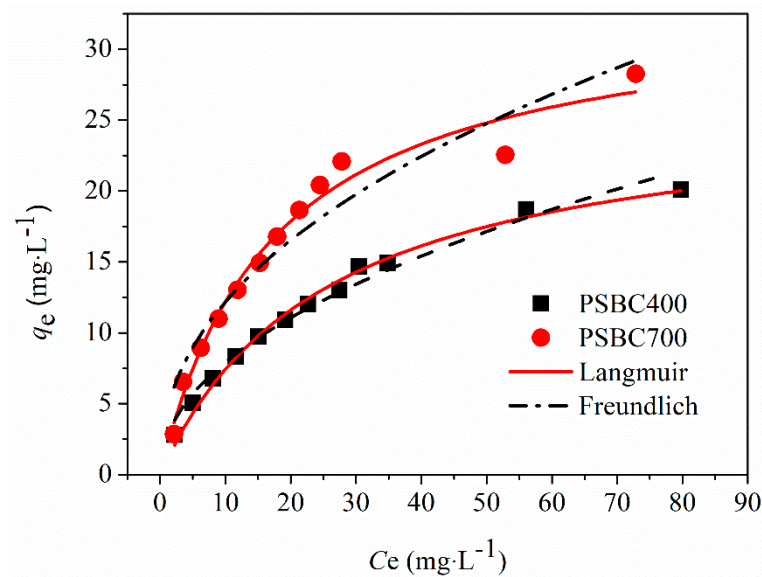


Figure 6. Adsorption isotherms of TC by biochars.

3.3. Adsorption Mechanism Analysis

(1) Pore-filling effect

The specific surface area and pore structure of a biochar play a key role in the adsorption of TC, principally determined by the pore-filling mechanism. Generally, a large surface area and well-developed pore structure in biochars result in a high adsorption capacity for TC [26,57]. In this study, PSBC700 is better at absorbing TC than PSBC400 because of its larger specific surface area and pore volume. The average pore size of PSBC 700 is 2.6512 nm, which is larger than the molecular size of TC (1.41 nm × 0.46 nm × 0.82 nm). Other studies also show that the pore-filling effect is responsible for the adsorption of TC onto the adsorbents [57,58]. The pore-filling effect is clearly shown to be a possible adsorption mechanism in this study.

(2) π - π interaction

The graphitized structure of a biochar also plays a major role in the adsorption of TC. The π - π interaction can occur between the graphitized structure (π -electron donor) of a biochar and the aromatic ring (π -electron acceptor) of TC molecules [59]. In this study, the H/C value and XRD analyses show that PSBC700 contains more graphitized carbon structures than PSBC400, suggesting that the π - π EDA interactions play a vital role in the TC adsorption process. Previous studies also show that π - π interactions are a key contributor to higher biochar TC adsorption capacity [36,60].

(3) Hydrogen bonding

In the adsorption process, hydrogen bonds usually play one of the most important roles. The surface O/N-containing functional groups of a biochar also play an important role in the adsorption of TC. Hydrogen bonds can be formed between the -OH (H-donor) on the adsorbent surface and the H acceptor (O atoms, N atoms, or aromatic rings of TC) [61]. The FTIR and XPS analyses show that PSBC400 has more functional groups than PSBC700, because some functional groups are retained at the lower pyrolysis temperature. Therefore, hydrogen bonding is an important interaction mechanism between PSBC400 and TC due to its high density of oxygen-containing groups. Other studies also show that a biochar can adsorb TC through hydrogen bonding, involving the -OH, C=O, and C-N functional groups [62].

(4) Surface complexation

Mineral components in a biochar can also bind with TC, mainly through surface complexation [63]. Based on the XRD, XRF, and XPS analyses, the amounts of Si, K, Ca, Al, and Fe in PSBC400 are greater than in PSBC700. Additionally, there are fewer mineral crystals in PSBC400 due to its lower pyrolysis temperature. Poor development of mineral crystals could provide more active sites onto which a pollutant can bind. Therefore, the minerals in PSBC400 play a crucial role in the adsorption of TC. Previous studies also show that minerals (such as Ca^{2+} and Mg^{2+}) on a biochar can efficiently adsorb TC through surface complexation [33,64] ($\text{Ca}^{2+} + \text{H}_2\text{TC}^- \rightleftharpoons \text{CaH}_2\text{TC}^+$; $\text{Ca}^{2+} + \text{HTC}^{2-} \rightleftharpoons \text{CaHTC}^0$; $\text{Mg}^{2+} + \text{H}_2\text{TC}^- \rightleftharpoons \text{MgH}_2\text{TC}^+$; $\text{Mg}^{2+} + \text{HTC}^{2-} \rightleftharpoons \text{MgHTC}^0$).

In summary, pyrolysis temperature significantly changes the dominant mechanism by which TC is adsorbed onto the two biochars. Specifically, the main mechanisms by which TC is adsorbed onto PSBC400 include hydrogen bonding and surface complexation, which are highly dependent on the functional groups (such as hydroxyl, carboxyl, amino, etc.) and minerals in a biochar. In contrast, pore filling and the π - π interaction may contribute to the possible mechanisms governing TC adsorption onto PSBC700 due to its surface area and graphitized carbon structure. A summary schematic illustration of the adsorption mechanisms of TC onto the two peanut shell biochars is presented in Figure 7.

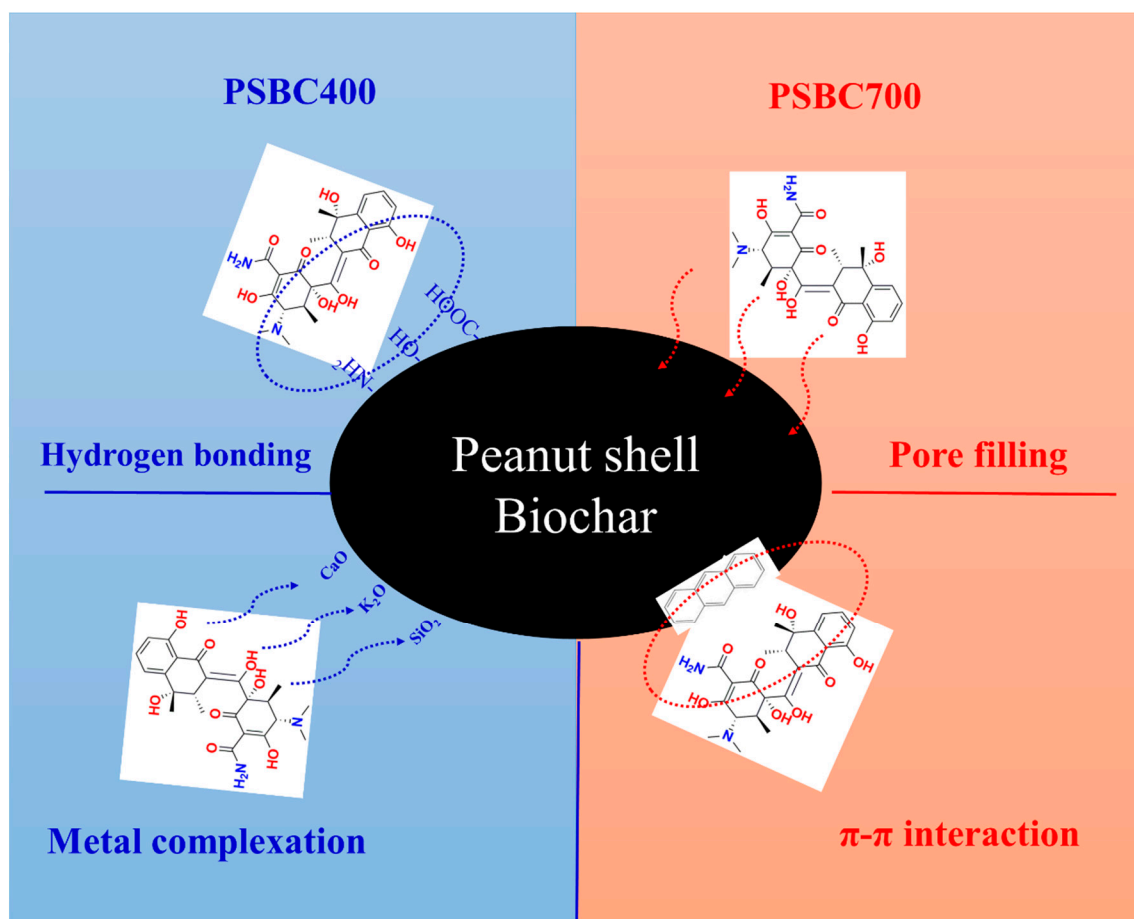


Figure 7. Schematic illustration of the adsorption mechanism between peanut shell biochar and TC.

4. Conclusions

Compared with PSBC400, PSBC700 shows a larger surface area and pore volume, and has higher carbon and ash contents, but lower amounts of O, N, and H. The hydrophilicity and polarity of PSBC700 is lower, but the aromaticity is higher. However, the mineral content of PSBC400 is greater than PSBC700. The functional groups in PSBC400 and

PSBC700 are different, especially the C- and O-related groups. The Elovich and the two-compartment adsorption kinetic models provide a good fit to the observed adsorption process of TC onto the two biochars. The Langmuir adsorption isotherm model provides a better description of the adsorption process of TC onto the two biochars. The theoretical maximum adsorption capacity of TC onto PSBC400 and PSBC700 reaches 26.4185 mg·g⁻¹ and 33.4346 mg·g⁻¹, respectively. The main adsorption mechanisms of TC onto PSBC400 are hydrogen bonding and complexation, and are related to its functional groups and minerals. In contrast, the main adsorption mechanisms of TC onto PSBC700 are pore filling and the π - π interaction, which are determined by its surface area and graphitized carbon structure.

Supplementary Materials: The following supporting information can be downloaded at: <https://www.mdpi.com/article/10.3390/su15010874/s1>, Table S1: Comparison of the adsorption capacity of TC on other pristine biochars [65]; Table S2: Comparison of the adsorption capacity of TC on other modified biochars.

Author Contributions: Conceptualization, S.F. and Y.W.; methodology, Z.S., Y.C., M.Z. and A.M.; software, Y.Z., Y.C., M.Z. and A.M.; validation, N.Z.; formal analysis, Y.Z.; investigation, S.F. and Y.W.; resources, Y.Z. and S.F.; data curation, Y.Z. and S.F.; writing—original draft preparation, Z.S., Y.Z.; writing—review and editing, S.F.; visualization, Z.S. and Y.Z.; supervision, N.Z.; project administration, S.F. and Y.W.; funding acquisition, S.F. and Y.W. All authors have read and agreed to the published version of the manuscript.

Funding: The research was funded by the National Natural Science Foundation of China (51809001, 32072464), Provincial Foundation for Excellent Young Talents of Colleges and Universities of Anhui Province (gxyq2021166), the Outstanding Youth Fund of Natural Science Foundation of Anhui Province (2208085Y07), and Undergraduate Innovation Project (202210364051).

Institutional Review Board Statement: Not applicable.

Informed Consent Statement: Not applicable.

Data Availability Statement: Not applicable.

Acknowledgments: The authors are grateful for financial support of the National Natural Science Foundation of China (51809001), Provincial Foundation for Excellent Young Talents of Colleges and Universities of Anhui Province (gxyq2021166), the Outstanding Youth Fund of Natural Science Foundation of Anhui Province (2208085Y07), and Undergraduate Innovation Project (202210364051).

Conflicts of Interest: The authors declare no conflict of interest.

References

1. Huang, H.; Zeng, S.; Dong, X.; Li, D.; Zhang, Y.; He, M.; Du, P. Diverse and abundant antibiotics and antibiotic resistance genes in an urban water system. *J. Environ. Manag.* **2019**, *231*, 494–503. [[CrossRef](#)] [[PubMed](#)]
2. Kovalakova, P.; Cizmas, L.; McDonald, T.J.; Marsalek, B.; Feng, M.; Sharma, V.K. Occurrence and toxicity of antibiotics in the aquatic environment: A review. *Chemosphere* **2020**, *251*, 126351. [[CrossRef](#)] [[PubMed](#)]
3. Xu, L.; Zhang, H.; Xiong, P.; Zhu, Q.; Liao, C.; Jiang, G. Occurrence, fate, and risk assessment of typical tetracycline antibiotics in the aquatic environment: A review. *Sci. Total Environ.* **2021**, *753*, 141975. [[CrossRef](#)] [[PubMed](#)]
4. Phoon, B.L.; Ong, C.C.; Mohamed Saheed, M.S.; Show, P.-L.; Chang, J.-S.; Ling, T.C.; Lam, S.S.; Juan, J.C. Conventional and emerging technologies for removal of antibiotics from wastewater. *J. Hazard. Mater.* **2020**, *400*, 122961. [[CrossRef](#)]
5. Ahmadijokani, F.; Molavi, H.; Tajahmadi, S.; Rezakazemi, M.; Amini, M.; Kamkar, M.; Rojas, O.J.; Arjmand, M. Coordination chemistry of metal–organic frameworks: Detection, adsorption, and photodegradation of tetracycline antibiotics and beyond. *Coord. Chem. Rev.* **2022**, *464*, 214562. [[CrossRef](#)]
6. Yang, R.T. *Adsorbents: Fundamentals and Applications*; John Wiley and Sons: Hoboken, NJ, USA, 2003; pp. 280–381. [[CrossRef](#)]
7. Mohan, D.; Sarswat, A.; Ok, Y.S.; Pittman, C.U. Organic and inorganic contaminants removal from water with biochar, a renewable, low cost and sustainable adsorbent—A critical review. *Bioresour. Technol.* **2014**, *160*, 191–202. [[CrossRef](#)]
8. Mei, Y.; Li, B.; Fan, S. Biochar from Rice Straw for Cu²⁺ Removal from Aqueous Solutions: Mechanism and Contribution Made by Acid-Soluble Minerals. *Water Air Soil Pollut.* **2020**, *231*, 420. [[CrossRef](#)]
9. Bian, S.; Xu, S.; Yin, Z.; Liu, S.; Li, J.; Xu, S.; Zhang, Y. An Efficient Strategy for Enhancing the Adsorption Capabilities of Biochar via Sequential KMnO₄-Promoted Oxidative Pyrolysis and H₂O₂ Oxidation. *Sustainability* **2021**, *13*, 2641. [[CrossRef](#)]

10. Chen, Y.; Li, L.; Wen, Q.; Yang, R.; Zhao, Y.; Rao, X.; Li, J.; Xu, S.; Song, H. Oxidative Magnetic Modification of Pristine Biochar Assisted by Ball-Milling for Removal of Methylene Blue and Tetracycline in Aqueous Solution. *Sustainability* **2022**, *14*, 9349. [[CrossRef](#)]
11. Kang, Z.; Jia, X.; Zhang, Y.; Kang, X.; Ge, M.; Liu, D.; Wang, C.; He, Z. A Review on Application of Biochar in the Removal of Pharmaceutical Pollutants through Adsorption and Persulfate-Based AOPs. *Sustainability* **2022**, *14*, 10128. [[CrossRef](#)]
12. Roy, H.; Islam, M.S.; Arifin, M.T.; Firoz, S.H. Synthesis, Characterization and Sorption Properties of Biochar, Chitosan and ZnO-Based Binary Composites towards a Cationic Dye. *Sustainability* **2022**, *14*, 14571. [[CrossRef](#)]
13. Wang, L.; Liu, S.; Xuan, W.; Li, S.; Wei, A. Efficient Nitrate Adsorption from Groundwater by Biochar-Supported Al-Substituted Goethite. *Sustainability* **2022**, *14*, 7824. [[CrossRef](#)]
14. Subedi, R.; Taupe, N.; Pelissetti, S.; Petruzzelli, L.; Bertora, C.; Leahy, J.J.; Grignani, C. Greenhouse gas emissions and soil properties following amendment with manure-derived biochars: Influence of pyrolysis temperature and feedstock type. *J. Environ. Manag.* **2016**, *166*, 73–83. [[CrossRef](#)]
15. Boguta, P.; Cybulak, M.; Sokołowska, Z.; Zarzycki, R.; Kacprzak, A.; Kobyłecki, R. Quality and quantity of humic-like and fulvic-like acids entrapped in biochars—The effect of various forestry feedstock and pyrolysis temperature of biochars. *Fuel* **2023**, *333*, 126405. [[CrossRef](#)]
16. Shan, R.; Shi, Y.; Gu, J.; Wang, Y.; Yuan, H. Single and competitive adsorption affinity of heavy metals toward peanut shell-derived biochar and its mechanisms in aqueous systems. *Chin. J. Chem. Eng.* **2020**, *28*, 1375–1383. [[CrossRef](#)]
17. Perea-Moreno, M.-A.; Manzano-Agugliaro, F.; Hernandez-Escobedo, Q.; Perea-Moreno, A.-J. Peanut Shell for Energy: Properties and Its Potential to Respect the Environment. *Sustainability* **2018**, *10*, 3254. [[CrossRef](#)]
18. Aryee, A.A.; Mpatani, F.M.; Kani, A.N.; Dovi, E.; Han, R.; Li, Z.; Qu, L. A review on functionalized adsorbents based on peanut husk for the sequestration of pollutants in wastewater: Modification methods and adsorption study. *J. Clean. Prod.* **2021**, *310*, 127502. [[CrossRef](#)]
19. Zhao, R.L.; Ma, X.X.; Xu, J.Q.; Zhang, Q.M. Removal of the Pesticide Imidacloprid from Aqueous Solution by Biochar Derived from Peanut Shell. *Bioresources* **2018**, *13*, 5656–5669. [[CrossRef](#)]
20. Yang, J.W.; Ji, G.Z.; Gao, Y.; Fu, W.; Irfan, M.; Mu, L.; Zhang, Y.L.; Li, A.M. High-yield and high-performance porous biochar produced from pyrolysis of peanut shell with low-dose ammonium polyphosphate for chloramphenicol adsorption. *J. Clean. Prod.* **2020**, *264*, 121516. [[CrossRef](#)]
21. Zhang, Y.; Xu, J.; Li, B.; Xie, Z.X.; Li, X.D.; Tang, J.; Fan, S.S. Enhanced adsorption performance of tetracycline in aqueous solutions by KOH-modified peanut shell-derived biochar. *Biomass Convers. Biorefin.* **2021**. [[CrossRef](#)]
22. Cai, W.Q.; Wei, J.H.; Li, Z.L.; Liu, Y.; Zhou, J.B.; Han, B.W. Preparation of amino-functionalized magnetic biochar with excellent adsorption performance for Cr(VI) by a mild one-step hydrothermal method from peanut hull. *Colloids Surf. A* **2019**, *563*, 102–111. [[CrossRef](#)]
23. An, Q.; Jiang, Y.Q.; Nan, H.Y.; Yu, Y.; Jiang, J.N. Unraveling sorption of nickel from aqueous solution by KMnO₄ and KOH-modified peanut shell biochar: Implicit mechanism. *Chemosphere* **2019**, *214*, 846–854. [[CrossRef](#)]
24. Han, X.Y.; Chu, L.; Liu, S.M.; Chen, T.M.; Ding, C.; Yan, J.L.; Cui, L.Q.; Quan, G.X. Removal of Methylene Blue from Aqueous Solution using Porous Biochar Obtained by KOH Activation of Peanut Shell Biochar. *Bioresources* **2015**, *10*, 2836–2849. [[CrossRef](#)]
25. Zhang, M.; Gao, B.; Yao, Y.; Xue, Y.W.; Inyang, M. Synthesis of porous MgO-biochar nanocomposites for removal of phosphate and nitrate from aqueous solutions. *Chem. Eng. J.* **2012**, *210*, 26–32. [[CrossRef](#)]
26. Li, B.; Zhang, Y.; Xu, J.; Fan, S.; Xu, H. Facile preparation of magnetic porous biochars from tea waste for the removal of tetracycline from aqueous solutions: Effect of pyrolysis temperature. *Chemosphere* **2022**, *291*, 132713. [[CrossRef](#)]
27. Hassan, M.; Liu, Y.; Naidu, R.; Parikh, S.J.; Du, J.; Qi, F.; Willett, I.R. Influences of feedstock sources and pyrolysis temperature on the properties of biochar and functionality as adsorbents: A meta-analysis. *Sci. Total Environ.* **2020**, *744*, 140714. [[CrossRef](#)]
28. Rodriguez, J.A.; Lustosa Filho, J.F.; Melo, L.C.A.; de Assis, I.R.; de Oliveira, T.S. Influence of pyrolysis temperature and feedstock on the properties of biochars produced from agricultural and industrial wastes. *J. Anal. Appl. Pyrolysis* **2020**, *149*, 104839. [[CrossRef](#)]
29. Ma, Z.; Yang, Y.; Ma, Q.; Zhou, H.; Luo, X.; Liu, X.; Wang, S. Evolution of the chemical composition, functional group, pore structure and crystallographic structure of bio-char from palm kernel shell pyrolysis under different temperatures. *J. Anal. Appl. Pyrolysis* **2017**, *127*, 350–359. [[CrossRef](#)]
30. Dai, Y.; Li, J.; Shan, D. Adsorption of tetracycline in aqueous solution by biochar derived from waste *Auricularia auricula* dregs. *Chemosphere* **2020**, *238*, 124432. [[CrossRef](#)] [[PubMed](#)]
31. Kim, J.E.; Bhatia, S.K.; Song, H.J.; Yoo, E.; Jeon, H.J.; Yoon, J.-Y.; Yang, Y.; Gurav, R.; Yang, Y.-H.; Kim, H.J.; et al. Adsorptive removal of tetracycline from aqueous solution by maple leaf-derived biochar. *Bioresour. Technol.* **2020**, *306*, 123092. [[CrossRef](#)]
32. Zhang, P.; Li, Y.; Cao, Y.; Han, L. Characteristics of tetracycline adsorption by cow manure biochar prepared at different pyrolysis temperatures. *Bioresour. Technol.* **2019**, *285*, 121348. [[CrossRef](#)] [[PubMed](#)]
33. Choi, Y.-K.; Choi, T.-R.; Gurav, R.; Bhatia, S.K.; Park, Y.-L.; Kim, H.J.; Kan, E.; Yang, Y.-H. Adsorption behavior of tetracycline onto *Spirulina* sp. (microalgae)-derived biochars produced at different temperatures. *Sci. Total Environ.* **2020**, *710*, 136282. [[CrossRef](#)] [[PubMed](#)]
34. Wang, Z.; Liu, G.; Zheng, H.; Li, F.; Ngo, H.H.; Guo, W.; Liu, C.; Chen, L.; Xing, B. Investigating the mechanisms of biochar's removal of lead from solution. *Bioresour. Technol.* **2015**, *177*, 308–317. [[CrossRef](#)] [[PubMed](#)]

35. Prasannamedha, G.; Kumar, P.S.; Mehala, R.; Sharumitha, T.J.; Surendhar, D. Enhanced adsorptive removal of sulfamethoxazole from water using biochar derived from hydrothermal carbonization of sugarcane bagasse. *J. Hazard. Mater.* **2021**, *407*, 124825. [[CrossRef](#)]
36. Jang, H.M.; Yoo, S.; Choi, Y.-K.; Park, S.; Kan, E. Adsorption isotherm, kinetic modeling and mechanism of tetracycline on Pinus taeda-derived activated biochar. *Bioresour. Technol.* **2018**, *259*, 24–31. [[CrossRef](#)] [[PubMed](#)]
37. Aljerf, L. High-efficiency extraction of bromocresol purple dye and heavy metals as chromium from industrial effluent by adsorption onto a modified surface of zeolite: Kinetics and equilibrium study. *J. Environ. Manag.* **2018**, *225*, 120–132. [[CrossRef](#)]
38. Ahmad, M.; Lee, S.S.; Dou, X.M.; Mohan, D.; Sung, J.K.; Yang, J.E.; Ok, Y.S. Effects of pyrolysis temperature on soybean stover- and peanut shell-derived biochar properties and TCE adsorption in water. *Bioresour. Technol.* **2012**, *118*, 536–544. [[CrossRef](#)]
39. Zhang, C.; Zhang, Z.; Zhang, L.; Li, Q.; Li, C.; Chen, G.; Zhang, S.; Liu, Q.; Hu, X. Evolution of the functionalities and structures of biochar in pyrolysis of poplar in a wide temperature range. *Bioresour. Technol.* **2020**, *304*, 123002. [[CrossRef](#)]
40. Xu, J.; Zhang, Y.; Li, B.; Fan, S.; Xu, H.; Guan, D.-X. Improved adsorption properties of tetracycline on KOH/KMnO₄ modified biochar derived from wheat straw. *Chemosphere* **2022**, *296*, 133981. [[CrossRef](#)]
41. Chen, D.; Yu, X.; Song, C.; Pang, X.; Huang, J.; Li, Y. Effect of pyrolysis temperature on the chemical oxidation stability of bamboo biochar. *Bioresour. Technol.* **2016**, *218*, 1303–1306. [[CrossRef](#)]
42. Xu, X.; Zhao, Y.; Sima, J.; Zhao, L.; Mašek, O.; Cao, X. Indispensable role of biochar-inherent mineral constituents in its environmental applications: A review. *Bioresour. Technol.* **2017**, *241*, 887–899. [[CrossRef](#)] [[PubMed](#)]
43. Zhang, C.; Chao, L.; Zhang, Z.; Zhang, L.; Li, Q.; Fan, H.; Zhang, S.; Liu, Q.; Qiao, Y.; Tian, Y.; et al. Pyrolysis of cellulose: Evolution of functionalities and structure of bio-char versus temperature. *Renew. Sustain. Energ. Rev.* **2021**, *135*, 110416. [[CrossRef](#)]
44. Nan, H.; Xiao, Z.; Zhao, L.; Yang, F.; Xu, H.; Xu, X.; Qiu, H. Nitrogen Transformation during Pyrolysis of Various N-Containing Biowastes with Participation of Mineral Calcium. *ACS Sustain. Chem. Eng.* **2020**, *8*, 12197–12207. [[CrossRef](#)]
45. Devi, P.; Saroha, A.K. Effect of pyrolysis temperature on polycyclic aromatic hydrocarbons toxicity and sorption behaviour of biochars prepared by pyrolysis of paper mill effluent treatment plant sludge. *Bioresour. Technol.* **2015**, *192*, 312–320. [[CrossRef](#)] [[PubMed](#)]
46. Guo, R.; Yan, L.; Rao, P.; Wang, R.; Guo, X. Nitrogen and sulfur co-doped biochar derived from peanut shell with enhanced adsorption capacity for diethyl phthalate. *Environ. Pollut.* **2020**, *258*, 113674. [[CrossRef](#)]
47. An, Q.; Li, Z.; Zhou, Y.; Meng, F.; Zhao, B.; Miao, Y.; Deng, S. Ammonium removal from groundwater using peanut shell based modified biochar: Mechanism analysis and column experiments. *J. Water Proc. Eng.* **2021**, *43*, 102219. [[CrossRef](#)]
48. Xu, Z.; Xu, X.; Tao, X.; Yao, C.; Tsang, D.C.W.; Cao, X. Interaction with low molecular weight organic acids affects the electron shuttling of biochar for Cr(VI) reduction. *J. Hazard. Mater.* **2019**, *378*, 120705. [[CrossRef](#)] [[PubMed](#)]
49. Wang, P.; Liu, X.; Yu, B.; Wu, X.; Xu, J.; Dong, F.; Zheng, Y. Characterization of peanut-shell biochar and the mechanisms underlying its sorption for atrazine and nicosulfuron in aqueous solution. *Sci. Total Environ.* **2020**, *702*, 134767. [[CrossRef](#)]
50. Chen, W.; Zhao, B.; Guo, Y.; Guo, Y.; Zheng, Z.; Pak, T.; Li, G. Effect of hydrothermal pretreatment on pyrolyzed sludge biochars for tetracycline adsorption. *J. Environ. Chem. Eng.* **2021**, *9*, 106557. [[CrossRef](#)]
51. Wang, B.; Zhai, Y.; Wang, T.; Li, S.; Peng, C.; Wang, Z.; Li, C.; Xu, B. Fabrication of bean dreg-derived carbon with high adsorption for methylene blue: Effect of hydrothermal pretreatment and pyrolysis process. *Bioresour. Technol.* **2019**, *274*, 525–532. [[CrossRef](#)]
52. Fan, S.; Wang, Y.; Wang, Z.; Tang, J.; Tang, J.; Li, X. Removal of methylene blue from aqueous solution by sewage sludge-derived biochar: Adsorption kinetics, equilibrium, thermodynamics and mechanism. *J. Environ. Chem. Eng.* **2017**, *5*, 601–611. [[CrossRef](#)]
53. Fan, S.; Tang, J.; Wang, Y.; Li, H.; Zhang, H.; Tang, J.; Wang, Z.; Li, X. Biochar prepared from co-pyrolysis of municipal sewage sludge and tea waste for the adsorption of methylene blue from aqueous solutions: Kinetics, isotherm, thermodynamic and mechanism. *J. Mol. Liquids* **2016**, *220*, 432–441. [[CrossRef](#)]
54. Betts, A.R.; Chen, N.; Hamilton, J.G.; Peak, D. Rates and Mechanisms of Zn²⁺ Adsorption on a Meat and Bonemeal Biochar. *Environ. Sci. Technol.* **2013**, *47*, 14350–14357. [[CrossRef](#)] [[PubMed](#)]
55. Bhagwat, G.; Tran, T.K.A.; Lamb, D.; Senathirajah, K.; Grainge, I.; O'Connor, W.; Juhasz, A.; Palanisami, T. Biofilms Enhance the Adsorption of Toxic Contaminants on Plastic Microfibers under Environmentally Relevant Conditions. *Environ. Sci. Technol.* **2021**, *55*, 8877–8887. [[CrossRef](#)] [[PubMed](#)]
56. Kypritidou, Z.; El-Bassi, L.; Jellali, S.; Kinigopoulou, V.; Tziritis, E.; Akrou, H.; Jeguirim, M.; Douglgeris, C. Lead removal from aqueous solutions by olive mill wastes derived biochar: Batch experiments and geochemical modelling. *J. Environ. Manag.* **2022**, *318*, 115562. [[CrossRef](#)] [[PubMed](#)]
57. Li, B.; Zhang, Y.; Xu, J.; Mei, Y.; Fan, S.; Xu, H. Effect of carbonization methods on the properties of tea waste biochars and their application in tetracycline removal from aqueous solutions. *Chemosphere* **2021**, *267*, 129283. [[CrossRef](#)] [[PubMed](#)]
58. Xiang, W.; Wan, Y.; Zhang, X.; Tan, Z.; Xia, T.; Zheng, Y.; Gao, B. Adsorption of tetracycline hydrochloride onto ball-milled biochar: Governing factors and mechanisms. *Chemosphere* **2020**, *255*, 127057. [[CrossRef](#)]
59. Ma, Y.; Li, M.; Li, P.; Yang, L.; Wu, L.; Gao, F.; Qi, X.; Zhang, Z. Hydrothermal synthesis of magnetic sludge biochar for tetracycline and ciprofloxacin adsorptive removal. *Bioresour. Technol.* **2021**, *319*, 124199. [[CrossRef](#)]
60. Liu, P.; Liu, W.-J.; Jiang, H.; Chen, J.-J.; Li, W.-W.; Yu, H.-Q. Modification of bio-char derived from fast pyrolysis of biomass and its application in removal of tetracycline from aqueous solution. *Bioresour. Technol.* **2012**, *121*, 235–240. [[CrossRef](#)]

61. Chen, Y.; Liu, J.; Zeng, Q.; Liang, Z.; Ye, X.; Lv, Y.; Liu, M. Preparation of *Eucommia ulmoides* lignin-based high-performance biochar containing sulfonic group: Synergistic pyrolysis mechanism and tetracycline hydrochloride adsorption. *Bioresour. Technol.* **2021**, *329*, 124856. [[CrossRef](#)]
62. Jang, H.M.; Kan, E. A novel hay-derived biochar for removal of tetracyclines in water. *Bioresour. Technol.* **2019**, *274*, 162–172. [[CrossRef](#)] [[PubMed](#)]
63. Mei, Y.; Xu, J.; Zhang, Y.; Li, B.; Fan, S.; Xu, H. Effect of Fe–N modification on the properties of biochars and their adsorption behavior on tetracycline removal from aqueous solution. *Bioresour. Technol.* **2021**, *325*, 124732. [[CrossRef](#)] [[PubMed](#)]
64. Zhang, X.; Li, Y.; Wu, M.; Pang, Y.; Hao, Z.; Hu, M.; Qiu, R.; Chen, Z. Enhanced adsorption of tetracycline by an iron and manganese oxides loaded biochar: Kinetics, mechanism and column adsorption. *Bioresour. Technol.* **2021**, *320*, 124264. [[CrossRef](#)] [[PubMed](#)]
65. Liu, H.; Xu, G.; Li, G. The characteristics of pharmaceutical sludge-derived biochar and its application for the adsorption of tetracycline. *Sci. Total Environ.* **2020**, *747*, 141492. [[CrossRef](#)]

Disclaimer/Publisher’s Note: The statements, opinions and data contained in all publications are solely those of the individual author(s) and contributor(s) and not of MDPI and/or the editor(s). MDPI and/or the editor(s) disclaim responsibility for any injury to people or property resulting from any ideas, methods, instructions or products referred to in the content.